PHOTONICS Research

Full-color micro-LED display with high color stability using semipolar (20-21) InGaN LEDs and quantum-dot photoresist

SUNG-WEN HUANG CHEN,[1] YU-MING HUANG,[1,2] KONTHOUJAM JAMES SINGH,[1] YU-CHIEN HSU,[1] FANG-JYUN LIOU,[1] JIE SONG,[3] JOOWON CHOI,[3] PO-TSUNG LEE,[1] CHIEN-CHUNG LIN,[2] ZHONG CHEN,[4] JUNG HAN,[5] TINGZHU WU,[4,6] AND HAO-CHUNG KUO[1,7]

[1]Department of Photonics & Graduate Institute of Electro-Optical Engineering, College of Electrical and Computer Engineering, Taiwan Chiao Tung University, Hsinchu 30010, China
[2]Institute of Photonic System, Taiwan Chiao Tung University, Tainan 71150, China
[3]Saphlux Inc., Branford, Connecticut 06405, USA
[4]Department of Electronic Science, Fujian Engineering Research Center for Solid-State Lighting, Xiamen University, Xiamen 361005, China
[5]Department of Electrical Engineering, Yale University, New Haven, Connecticut 06520, USA
[6]e-mail: wutingzhu@xmu.edu.cn
[7]e-mail: hckuo@faculty.nctu.edu.tw

Received 22 January 2020; revised 19 February 2020; accepted 5 March 2020; posted 5 March 2020 (Doc. ID 388958); published 15 April 2020

Red-green-blue (RGB) full-color micro light-emitting diodes (μ-LEDs) fabricated from semipolar (20-21) wafers, with a quantum-dot photoresist color-conversion layer, were demonstrated. The semipolar (20-21) InGaN/GaN μ-LEDs were fabricated on large (4 in.) patterned sapphire substrates by orientation-controlled epitaxy. The semipolar μ-LEDs showed a 3.2 nm peak wavelength shift and a 14.7% efficiency droop under 200 A/cm² injected current density, indicating significant amelioration of the quantum-confined Stark effect. Because of the semipolar μ-LEDs' emission-wavelength stability, the RGB pixel showed little color shift with current density and achieved a wide color gamut (114.4% NTSC space and 85.4% Rec. 2020). © 2020 Chinese Laser Press

https://doi.org/10.1364/PRJ.388958

1. INTRODUCTION

Micro light-emitting diodes (μ-LEDs) are considered the most promising light sources for next-generation display technology [1–5], with many performance advantages over technologies in current use. By assembling red-green-blue (RGB) μ-LEDs into matrices through the mass-transfer process, it is possible to achieve full-color displays [6–9]. However, the mass-transfer process remains challenging owing to its low transfer yield, slow throughput, and high fabrication cost [10–12]. Color conversion based on quantum dots (QDs), which requires only blue or UV LEDs as a lighting source, has been suggested as a way to reduce the difficulty of the mass-transfer process [13,14]. Commercially available blue or UV LEDs are normally grown on conventional (0001) "polar" *c*-plane sapphire substrates; further, the epitaxial technology of *c*-plane gallium nitride (GaN) based LEDs has become quite mature over the past few decades [15,16]. Unfortunately, LEDs fabricated on *c*-plane substrates suffer from a droop (efficiency reduction) and emission wavelength shift caused by the quantum confined Stark effect (QCSE) [17,18]. The QCSE is a result of the built-in electrical field caused by the polarization field. GaN is a hexagonal crystal with wurtzite symmetry, the highest symmetry compatible with spontaneous piezoelectric polarization [19]. Furthermore, a large piezoelectric field (on the order of MV/cm) can be induced in the multiple quantum well (MQW) strained layers in the LED structure [20]. These internal polarization fields along the *c* plane (*z* axis) result in the accumulation of charge at the heterojunction of the quantum barrier and quantum well, further tilting the energy bandgap and also causing a spatial separation between the wave-function distributions of holes and electrons. A redshift of the emission wavelength and a decrease in the transition probability are thus produced. As *c*-plane-grown GaN materials are subject to strong built-in electric fields because of spontaneous and piezoelectric polarization, LEDs based on *c*-plane epitaxial wafers can only operate at low current densities owing to the significant decrease of efficiency as the current density increases. Low efficiency and wide-range color shifts are undesired features in displays the other applications [21,22]. The common approach to addressing the problem of the QCSE in *c*-plane epitaxy is to insert a strain-relief layer before the multiple quantum well layer during the epitaxial process [23,24], but this method can only eliminate a small proportion of QCSE. A better way to ameliorate the disadvantage caused by QCSE is to start by addressing the

fundamental problem, that is, the origin of the polarization field in the crystal plane. Growing III-nitride LED devices on semipolar orientations is an additional approach to droop reduction, one that circumvents the issues associated with polarization-related electric fields in conventional *c*-plane structures [25,26].

Colloidal QDs exhibit excellent photoluminescence (PL) characteristics, originating with the quantum confinement effect, and are suitable for use as a color-conversion layer for μ-LEDs [27,28]. Combined with a color filter on top of QDs, the QD-based μ-LED display can achieve a high contrast ratio [13,29]. An alternative method of mass producing high-resolution μ-LED displays and overcoming mass-transfer technical difficulties is the photolithography process currently being applied to patterning large-area devices [30,31]. QDs can be combined with photoresist (PR) to form QDPR after surface modification [30]. QDPR provides an approach to patterning multicolor QD arrays with the ability to control thickness and size while retaining the advantages of photolithography. This method provides a cost-efficient, practical solution to the bottlenecks in developing high-resolution, large-area devices, especially full-color μ-LEDs for display applications.

This study reports a full-color μ-LED array with high color stability that is fabricated from semipolar (20-21) blue LEDs with a 50 μm diameter chip size and a green or red QDPR color-conversion layer. It is the demonstration that innovatively achieves full-color display through the semipolar μ-LED device, while past studies generally discuss the wavelength stability in a single color. Compared to *c*-plane LEDs with a similar MQW design, semipolar (20-21) μ-LEDs show much better wavelength-shift characteristics and an improved efficiency droop. Red and green pixels manufactured with QDPR can significantly filter blue light to improve color purity. Moreover, the use of the black photoresist matrix achieves high contrast and avoids the effect of cross-talk [32]. This technique illustrates the color stability of μ-LED, thereby eliminating doubts about its applicability to displays.

2. EXPERIMENT

The first step in the experiment was the metal-organic chemical vapor deposition (MOCVD) growth of a (20-21)-oriented GaN layer on a specific patterned sapphire substrate (PSS). Traditionally, semipolar GaN is produced by the off-axis slicing of bulk-form hydride vapor-phase epitaxy grown (HVPE-grown) GaN substrates, which are expensive and physically incompatible with mass production [33,34]. In the present experiment, an innovative orientation-controlled epitaxy (OCE) process with semipolar GaN material selectively grown directly on the standard sapphire wafer was used to overcome this problem. A simple epitaxial method involving MOCVD with a sidewall of trench-etched substrates produced stacking-fault (SF) free semipolar GaN upon coalescence. For details on the PSS and bulk GaN epitaxy, please refer to our previous research results [35,36]. The epitaxial structure consisted of a bulk GaN buffer layer (5 μm), an n-GaN layer (1.5 μm), an undoped InGaN/GaN MQW active layer, a p-GaN layer (150 nm), and a p-InGaN layer (3 nm). The MQWs were constructed using five pairs of 3 nm thick InGaN wells and a 5 nm thick GaN barrier with an emission wavelength around 450 nm. The *c*-plane wafer in this study was designed with a similar MQW structure.

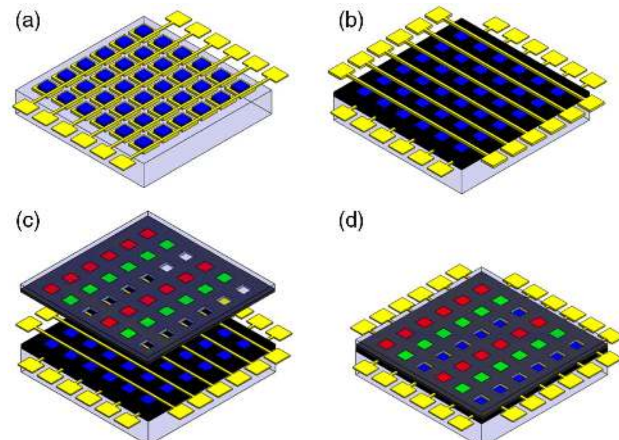

Fig. 1. Process flow for the fabrication of a full-color RGB pixel array. (a) μ-LED array process. (b) Black PR matrices and p-electrode metal lines. (c) Red, green, and blue (transparent) pixel lithography process. (d) Color pixel bonding.

The μ-LED array process began with the deposition of a transparent conducting oxide (TCO) layer, followed by annealing at 450°C for 2 min by rapid thermal annealing under ambient atmospheric conditions to form a p-type ohmic contact. Next, a HCl solution and inductively coupled plasma-reactive ion etching (ICP-RIE) were used to etch the TCO film and to perform a 1 μm depth mesa etch, respectively. Subsequently, Ti/Al/Ti/Au (20 nm/150 nm/10 nm/100 nm) layers were deposited through electron beam evaporation to act as the n-type electrode. After that, a 200 nm thick SiO_2 passivation layer was deposited by plasma-enhanced chemical vapor deposition. Last, the via-hole process, followed by ICP-RIE, was used to complete the μ-LED array. Figure 1 schematically illustrates the lithographic process of black PR matrices and QDPR on the semipolar μ-LED array. A black photoresist was used to flatten the μ-LED array and prevent the lateral leakage of blue light. Then, the Ni/Au (p-electrode metal) lines were deposited on the flattened surface to link each chip, as shown in Fig. 1(b). Next, the gray photoresist, red QDPR, green QDPR, and transparent PR were fabricated by the lithography process sequentially to form a color pixel on a highly-transparent glass substrate with 0.7 mm thickness, as shown in Fig. 1(c). The color pixel size is designed at 80 μm × 80 μm with 30 μm spacing between each pixel. Finally, in Fig. 1(d), the color pixel array on glass was stuck together with μ-LED array by using an aligner and UV resin.

3. RESULTS AND DISCUSSION

A large-area semipolar GaN grown on a patterned sapphire substrate by OCE can, in theory achieve, all crystal planes by controlling the inclined sidewalls [37]. Figure 2 presents a series of images of a 4 in., SF-free (20-21) blue LED epitaxial wafer. The semipolar heteroepitaxy process starts by patterning the sapphire substrates into stripe trenches and depositing a SiO_2 mask

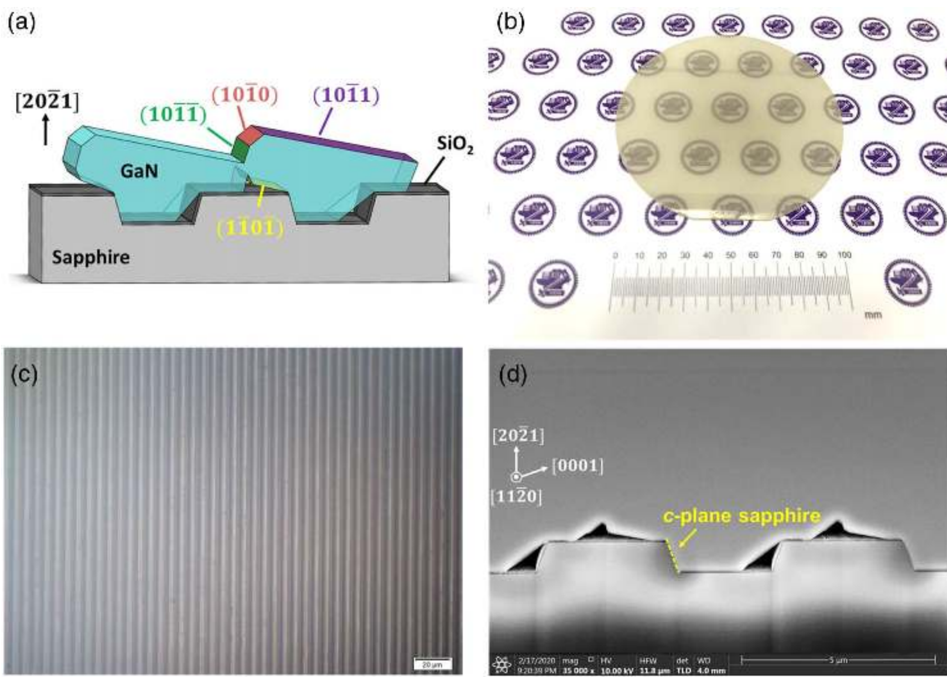

Fig. 2. (a) Schematic diagram of the semipolar GaN grown on a patterned sapphire substrate. (b) Photograph of a 4 in. wafer of SF-free (20-21) InGaN/GaN LED grown on a patterned sapphire substrate. (c) Top-view microscopy image of SF-free (20-21) InGaN/GaN LED grown on a patterned sapphire substrate. (d) Cross-sectional SEM image of (20-21) GaN grown on a patterned sapphire substrate by orientation-controlled epitaxy.

to cover the surface of the PSS beyond the selected *c*-plane sidewall. Then, GaN is grown selectively on exposed sidewalls of the PSS until the stripes coalesce into a thick, continuous semipolar GaN film. Further, the GaN crystal will be bounded by (10-11), (10-10), (10-1-1), and (1-10-1) facets, as shown in Fig. 2(a). The semipolar (20-21) facet can only exist after the semipolar GaN template is polished by the chemical–mechanical planarization process, as the semipolar (20-21) facet is an artificial plane and cannot appear naturally in the epitaxial process. In Fig. 2(b), the logo of Taiwan Chiao Tung University is clearly visible through the epitaxial wafer. This high degree of transparency indicates the uniformity and low-defect density of the epitaxial structures. Figures 2(c) and 2(d) show an optical-microscope image and a scanning electron microscope (SEM) cross-sectional image of the semipolar LED epitaxial layer. Each stripe shown in Fig. 2(c) is approximately 3 μm wide, with a pitch of 6 μm and 1 μm depth. The SEM image [Fig. 2(d)] marks the crystalline facet of GaN with surface normal direction toward GaN [20-21] and illustrates that neighboring GaN crystals coalesce well.

The optical-electrical characteristics of μ-LED devices are summarized in Fig. 3, along with the results of numerical simulations. (The physical modeling in this study was conducted using APSYS, produced by Crosslight Software Inc.) Figure 3(a) shows the current density-voltage (*J-V*) characteristic of a semipolar μ-LED with a 50 μm diameter chip; the inset is the image of lighting from semipolar μ-LEDs. A forward voltage of 3.2 V at 20 A/cm^2 indicates electrical properties comparable with those of common *c*-plane devices. The electroluminescence (EL) spectrum at various current densities is shown in Fig. 3(b). The EL spectrum shows a 453 nm peak wavelength and 24.8 nm full width at half maximum (FWHM) under the 200 A/cm^2 driving condition. The narrow FWHM indicates good quality of semipolar epitaxy, comparable with that of common *c*-plane devices. Figure 3(c) shows the experimental data and numerical fit for the external quantum efficiency (EQE) of semipolar and *c*-plane devices. There is good agreement between the experimental data and the simulation. The *c*-plane device shows the larger (~1.7 times) maximum EQE than the semipolar μ-LED by the experiment data. Despite this, the output power produced by the semipolar device is sufficient to support the color conversion in this work. Moreover, a good value of EQE is retained by the semipolar device even at a high injected current density of 200 A/cm^2, with only 14.7% droop, whereas the *c*-plane device exhibits a droop over 55% under the same conditions. The output power and EQE of semipolar devices can be further improved through the optimization of the active area in the future.

Carrier leakage and Auger recombination have been the most frequently proposed mechanisms for explaining the origin of the efficiency droop in past studies [38–40]; these mechanisms cause droop because QCSE leads to a low carrier recombination rate. From the simulation, the Auger recombination coefficients of semipolar and *c*-plane structures are 1×10^{-30} cm^6/s and 4.5×10^{-30} cm^6/s, respectively. These values are similar to those found in the literature and explain one of the reasons that affect a serious droop in *c*-plane devices [39,41–43].

The polarization charges that accumulate at the hetero interfaces of the active region cause energy-band tilting and separate the overlap of the wave-function distribution. This is the

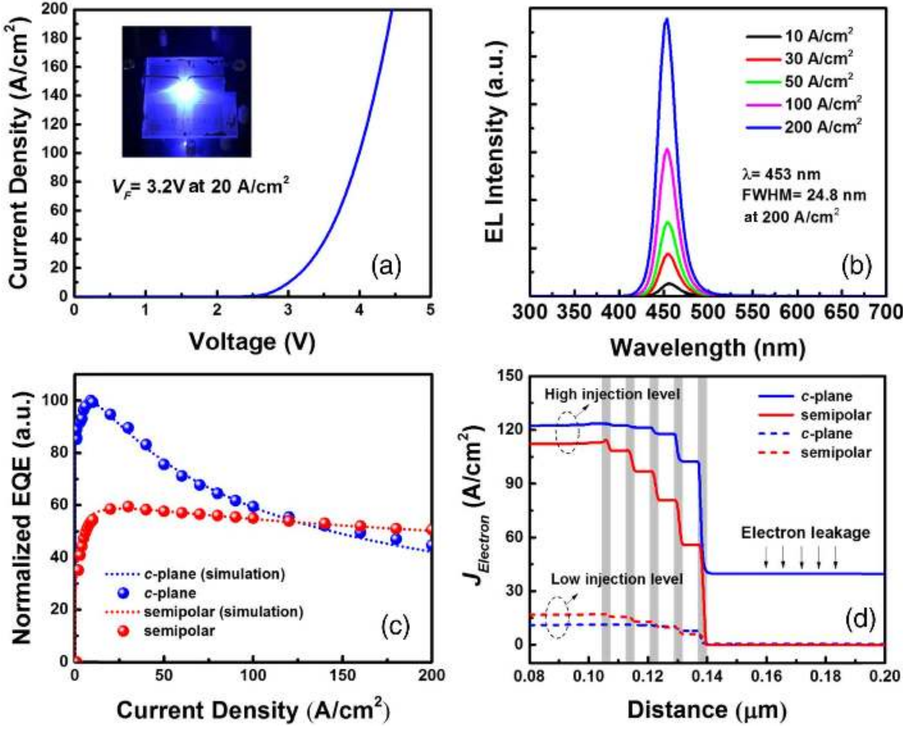

Fig. 3. (a) *J-V* curve of semipolar μ-LEDs, with image of lighting from device. (b) Electroluminescence spectrum of semipolar μ-LED with increasing applied current density. (c) Experimental data and simulation curves for normalized external quantum efficiency of semipolar and *c*-plane μ-LEDs. (d) Simulated electron current density throughout whole semipolar and *c*-plane μ-LED structures at 20 A/cm^2 and 200 A/cm^2 forward current density.

main reason for nonradiative recombination and carrier leakage. Furthermore, the number of electrons in QW is much higher than the number of holes, indicating that the carrier leakages are dominated by the electron overflow. Figure 3(d) shows the simulated electron current density of 20 A/cm^2 and 200 A/cm^2 throughout the whole semipolar LED structure as well as the *c*-plane LED structure. The gray areas marked in Fig. 3(d) are the position of QWs. The leftover electron density after five pairs of QWs is regarded as the electron overflow or electron leakage. Due to the lower recombination efficiency, the stepwise decline cannot be clearly observed in *c*-plane device. Additionally, because of the QCSE, the MQWs in *c*-plane devices cannot effectively generate carrier recombination, so the electron density cannot be significantly reduced after the electron current passing through the first three pairs of QWs. The electron density is greatly reduced at the last two pairs of QWs since the electron current is close to the p-GaN region in which a much higher density of hole exists. In contrast, the electrons can be efficiently recombined in every QW in the semipolar device, which indicates the mitigation of the QCSE. This simulation result shows serious electron overflow in the *c*-plane LED with the high injection level compared with the semipolar LED. Both Auger recombination and carrier leakage (electron overflow) are responsible for the severe efficiency droop and as is clear from the simulation results.

An image of RGB pixel matrices on glass obtained through fluorescence microscopy (FLOM) is shown in Fig. 4(a). The FLOM image illustrates the high contrast ratio between the gray PR matrices and the color pixels. Compared with the bottom black PR used to reduce blue-light side leakage, the gray PR mold can attain a higher height (6–10 μm) and provide higher reflectivity, thus reducing the cross-talk effect among pixels and enhancing output intensity by inside reflection. Figure 4(b) shows the overlap of the EL spectrum of the semipolar μ-LED and the absorption spectra of the green and red QDPRs. It can be observed from the curves that red and green QDPRs absorb a certain amount of blue light from semipolar μ-LEDs and thus can be used for color conversion. The QDPR used in this study consists of a specific photoresist, colloidal QD solvent (25 wt%), and TiO_2 powder in a 3:1:0.1 volume ratio. The ratio of each material will influence the performance of QDPR; for instance, a higher QD ratio can enhance the conversion efficiency, but the critical pattern linewidth may change [44]. We use CdSe/CdZnS-based thick-shell QDs, which have 85% photoluminescent quantum yield (PLQY) as the phosphor material; further, the brightness of the display depends on the film EQE (i.e., $\text{EQE} \approx \text{PLQY}_{\text{QD-film}} \times$ light extraction efficiency) of QDPR [44]. Therefore, for our red and green QDs, their EQEs are 51% and 38%, considering that their light extraction efficiencies are about 60% and 45%, respectively. TiO_2 can be regarded as a reflector of incident light in QDPR and further improves the absorption of emission light by QDs. The electroluminescence spectra of red and green pixels driving at 200 A/cm^2 with the QDPR thickness of 6 μm are shown in Fig. 4(c). The red and green pixels show peak wavelengths of 630 and 536 nm, respectively.

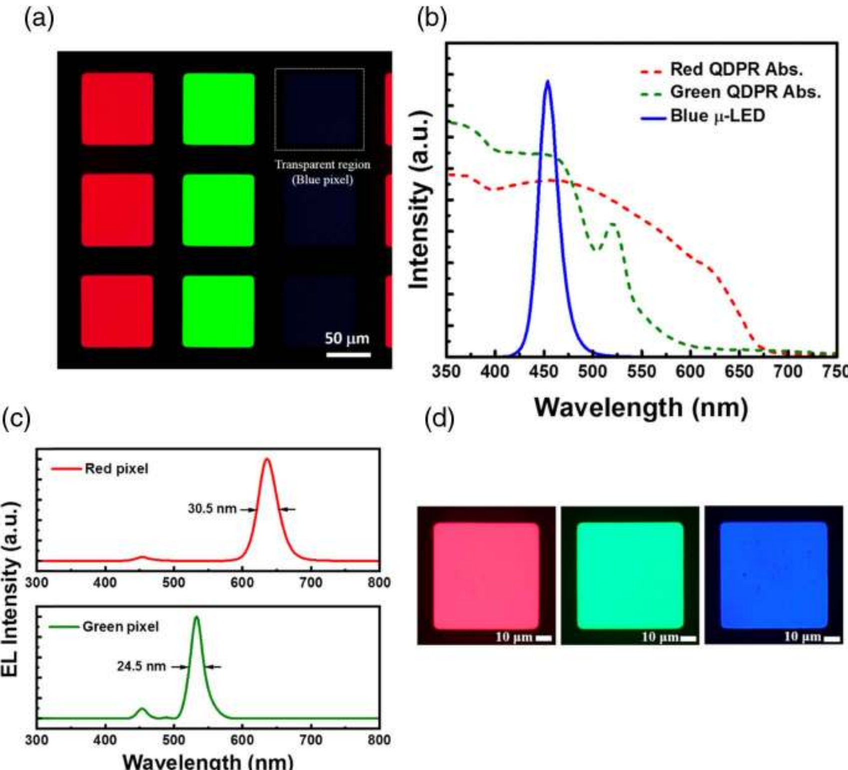

Fig. 4. (a) Fluorescence microscopy image of RGB pixel. (b) Overlap relationship between blue μ-LED electroluminescence emission and absorption of quantum-dot photoresist. (c) Electroluminescence spectra of red and green pixels. (d) Electroluminescence microscope image of RGB pixels.

According to the EL spectra of semipolar μ-LEDs shown in Fig. 3(b), the RGB emission spectra have FWHMs of 30.5, 24.5, and 24.8 nm, respectively. These values imply good performance in color rendering. These spectra also illustrate that, under the 6 μm thick QDPR, most of the blue light has been absorbed. Blue light leakage can be reduced for practical applications by increasing the QDPR thickness or changing the composition of the QDPR. Figure 4(d) shows the electroluminescence microscope image of the RGB pixel at 200 A/cm^2 driving condition. Because of the leakage reduced from bottom black photoresist, top gray photoresist matrices, and the only remaining blue light from QD pixel, each pixel shows vivid color individually.

Figure 5 presents the statistical peak wavelengths for *c*-plane and semipolar μ-LEDs with driving conditions of 1 to 200 A/cm^2. The *c*-plane and semipolar μ-LEDs show peak wavelength shifts of 13.0 and 3.2 nm, respectively. The peak wavelength of the semipolar device was stable after 30 A/cm^2 and no longer shifted, but the *c*-plane device only became stable after reaching 90 A/cm^2. The semipolar device exhibited a smaller peak wavelength shift and faster stabilization with applied current density, which can be attributed to the reduction of the polarization field by the semipolar structure and improved energy band tilt.

Next, Fig. 6 demonstrates the color performance of RGB μ-LEDs under 1 to 200 A/cm^2 driving conditions in the CIE 1931 and CIE 1976. As we know, CIE 1976 can provide a more uniform color spacing than CIE 1931 [45]. For *c*-plane

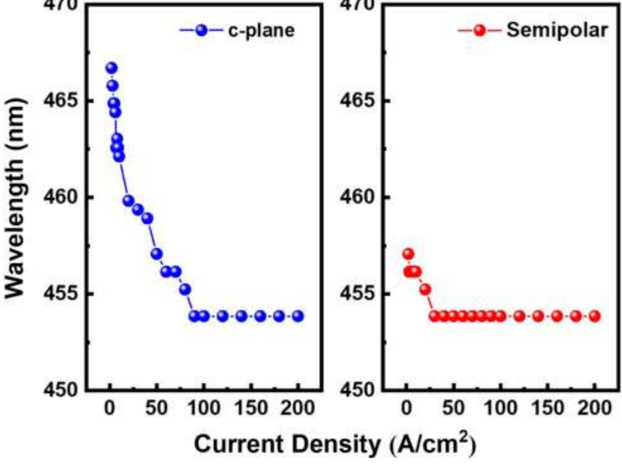

Fig. 5. Peak wavelengths of *c*-plane and semipolar μ-LEDs in range 1 to 200 A/cm^2 current density.

and semipolar blue μ-LEDs, the color coordinates varied from (0.1572, 0.1067) to (0.1483, 0.0379) and (0.1433, 0.0388) to (0.1490, 0.0317) in the CIE 1931 chromaticity diagram, and the color shift ($\Delta\mu'\nu'$) was 0.1374 and 0.0209 in the CIE 1976, respectively. A color gamut comparison of *c*-plane and semipolar RGB pixels is also presented in Fig. 6. The color gamut of the RGB pixel assembled from semipolar μ-LEDs was almost unchanged owing to the wavelength stability, while

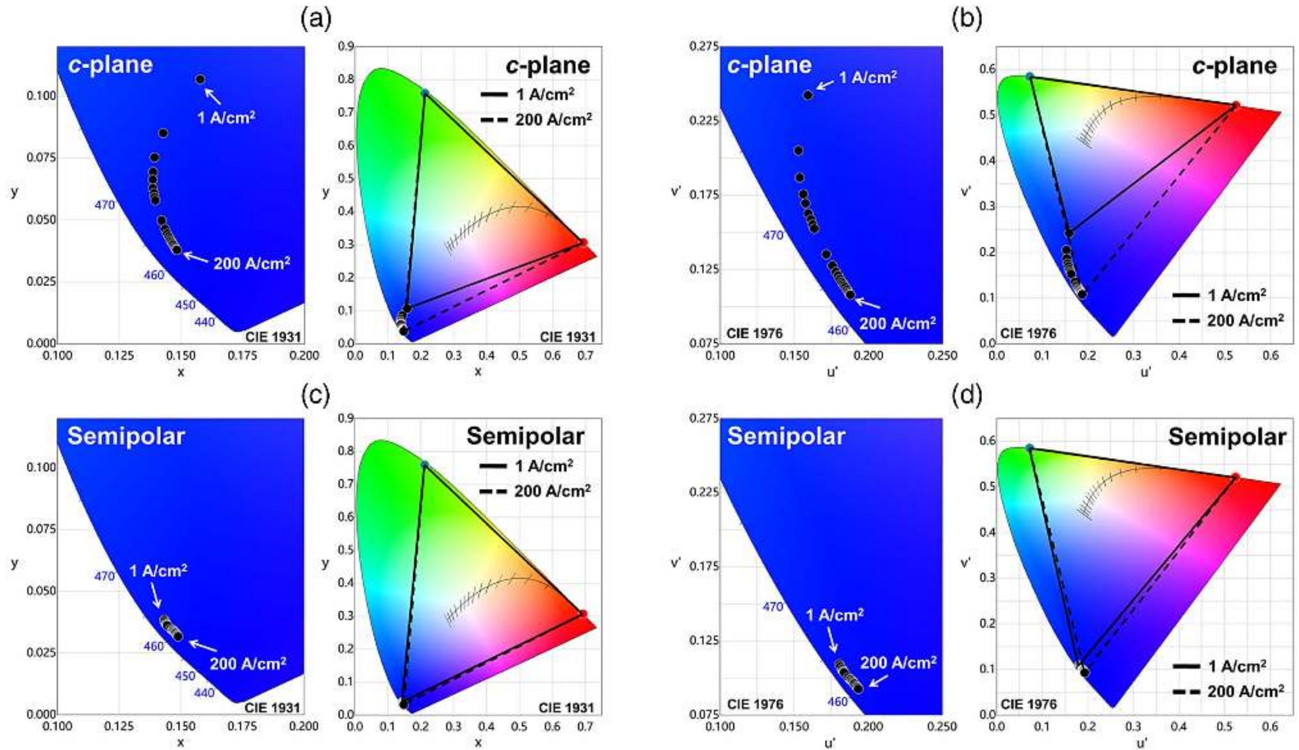

Fig. 6. Color gamut of RGB pixel assembly from *c*-plane μ-LED and QDPR under various current densities in (a) CIE 1931 and (b) CIE 1976. Color gamut of RGB pixel assembly from semipolar μ-LED and QDPR under various current densities in (c) CIE 1931 and (d) CIE 1976.

c-plane devices had a 10% variation (in the CIE 1931) as the applied current density increased. The red and green pixels also showed almost no color shift owing to emission by optical pumping and the stabilizing material characteristics of QDPR. Furthermore, the RGB pixel assembled from semipolar μ-LEDs and QDPR demonstrated wide color-gamut characteristics because of its narrow EL spectrum; it achieved 114.4% of National Television Standards Committee (NTSC) space and 85.4% Rec. 2020 in the CIE 1931. The RGB full-color devices assembled from semipolar μ-LEDs with QDPR proposed in this study show excellent color stability and wide color-gamut characteristics, showing great promise for display applications.

4. CONCLUSION

In conclusion, semipolar (20-21) μ-LEDs and a QDPR lithography process have been used to produce an RGB full-color μ-LED device. The SF-free semipolar LED is grown on PSS, which is inexpensive and has a large area; its properties are comparable with those of a *c*-plane LED, which indicates its good epitaxial quality. The semipolar μ-LED shows a stabilizing wavelength shift of 3.2 nm compared with the *c*-plane μ-LED's shift of 13.0 nm. These results make it an attractive candidate light source for display applications. A color-conversion layer formed by QDPR is suitable for the common lithography process and thus for large-scale manufacturing. Finally, the RGB pixels present a wide color gamut of 114.4% NTSC and 85.4% Rec. 2020, with high color stability determined by the variation of the color gamut.

Funding. Ministry of Science and Technology, Taiwan, China (107-2221-E-009-113-MY3, 108-2221-E-009-113-MY3); National Natural Science Foundation of China (11904302); Hsinchu Science Park Bureau, Ministry of Science and Technology, Taiwan, China (108A08B); Major Science and Technology Project of Xiamen, China (3502Z20191015).

Acknowledgment. The authors would like to thank Mr. Kuan-An Chen from Synth-Edge Advanced Materials Co., Ltd. for technical supporting in quantum-dots photoresist.

REFERENCES

1. Z. J. Liu, W. C. Chong, K. M. Wong, and K. M. Lau, "360 PPI flip-chip mounted active matrix addressable light emitting diode on silicon (LEDoS) micro-displays," J. Disp. Technol. **9**, 490–496 (2013).
2. Z. Gong, E. Gu, S. R. Jin, D. Massoubre, B. Guilhabert, H. X. Zhang, M. D. Dawson, V. Poher, G. T. Kennedy, P. M. W. French, and M. A. A. Neil, "Efficient flip-chip InGaN micro-pixellated light-emitting diode arrays: promising candidates for micro-displays and colour conversion," J. Phys. D **41**, 094002 (2008).
3. T. Wu, C.-W. Sher, Y. Lin, C.-F. Lee, S. Liang, Y. Lu, S.-W. H. Chen, W. Guo, H.-C. Kuo, and Z. Chen, "Mini-LED and micro-LED: promising candidates for the next generation display technology," Appl. Sci. **8**, 1557 (2018).
4. G. J. Tan, Y. G. Huang, M. C. Li, S. L. Lee, and S. T. Wu, "High dynamic range liquid crystal displays with a mini-LED backlight," Opt. Express **26**, 16572–16584 (2018).
5. Y. Huang, G. Tan, F. Gou, M. C. Li, S. L. Lee, and S. T. Wu, "Prospects and challenges of mini-LED and micro-LED displays," J. Soc. Inf. Disp. **27**, 387–401 (2019).
6. C.-H. Lin, A. Verma, C.-Y. Kang, Y.-M. Pai, T.-Y. Chen, J.-J. Yang, C.-W. Sher, Y.-Z. Yang, P.-T. Lee, C.-C. Lin, Y.-C. Wu, S. K. Sharma, T. Wu, S.-R. Chung, and H.-C. Kuo, "Hybrid-type white LEDs based

on inorganic halide perovskite QDs: candidates for wide color gamut display backlights," Photon. Res. **7**, 579–585 (2019).
7. H.-S. Kim, E. Brueckner, J. Song, Y. Li, S. Kim, C. Lu, J. Sulkin, K. Choquette, Y. Huang, R. G. Nuzzo, and J. A. Rogers, "Unusual strategies for using indium gallium nitride grown on silicon (111) for solid-state lighting," Proc. Natl. Acad. Sci. USA **108**, 10072–10077 (2011).
8. V. Marinov, O. Swenson, R. Miller, F. Sarwar, Y. Atanasov, M. Semler, and S. Datta, "Laser-enabled advanced packaging of ultrathin bare dice in flexible substrates," IEEE Trans. Compon. Packag. Technol. **2**, 569–577 (2012).
9. K. Ding, V. Avrutin, N. Izyumskaya, U. Ozgur, and H. Morkoc, "Micro-LEDs, a manufacturability perspective," Appl. Sci. **9**, 1206 (2019).
10. M. Meitl, E. Radauscher, S. Bonafede, D. Gomez, T. Moore, C. Prevatte, B. Raymond, B. Fisher, K. Ghosal, and A. Fecioru, "Passive matrix displays with transfer-printed microscale inorganic LEDs," in *SID Symposium Digest of Technical Papers* (Wiley, 2016), pp. 743–746.
11. L. Zhang, F. Ou, W. C. Chong, Y. Chen, and Q. Li, "Wafer-scale monolithic hybrid integration of Si-based IC and III-V epi-layers–a mass manufacturable approach for active matrix micro-LED micro-displays," J. Soc. Inf. Disp. **26**, 137–145 (2018).
12. R. S. Cok, M. Meitl, R. Rotzoll, G. Melnik, A. Fecioru, A. J. Trindade, B. Raymond, S. Bonafede, D. Gomez, T. Moore, C. Prevatte, E. Radauscher, S. Goodwin, P. Hines, and C. A. Bower, "Inorganic light-emitting diode displays using micro-transfer printing," J. Soc. Inf. Disp. **25**, 589–609 (2017).
13. H.-V. Han, H.-Y. Lin, C.-C. Lin, W.-C. Chong, J.-R. Li, K.-J. Chen, P. Yu, T.-M. Chen, H.-M. Chen, K.-M. Lau, and H.-C. Kuo, "Resonant-enhanced full-color emission of quantum-dot-based micro LED display technology," Opt. Express **23**, 32504–32515 (2015).
14. S.-W. Huang Chen, C.-C. Shen, T. Wu, Z.-Y. Liao, L.-F. Chen, J.-R. Zhou, C.-F. Lee, C.-H. Lin, C.-C. Lin, C.-W. Sher, P.-T. Lee, A.-J. Tzou, Z. Chen, and H.-C. Kuo, "Full-color monolithic hybrid quantum dot nanoring micro light-emitting diodes with improved efficiency using atomic layer deposition and nonradiative resonant energy transfer," Photon. Res. **7**, 416–422 (2019).
15. S. Nakamura, N. Senoh, N. Iwasa, and S. I. Nagahama, "High-brightness InGaN blue, green and yellow light-emitting-diodes with quantum-well structures," Jpn. J. Appl. Phys. **34**, L797–L799 (1995).
16. Y. J. Lee, J. M. Hwang, T. C. Hsu, M. H. Hsieh, M. J. Jou, B. J. Lee, T. C. Lu, H. C. Kuo, and S. C. Wang, "Enhancing the output power of GaN-based LEDs grown on wet-etched patterned sapphire substrates," IEEE Photon. Tech. Lett. **18**, 1152–1154 (2006).
17. T. Takeuchi, S. Sota, M. Katsuragawa, M. Komori, H. Takeuchi, H. Amano, and I. Akasaki, "Quantum-confined stark effect due to piezoelectric fields in GaInN strained quantum wells," Jpn. J. Appl. Phys. **36**, L382–L385 (1997).
18. T. Takeuchi, C. Wetzel, S. Yamaguchi, H. Sakai, H. Amano, I. Akasaki, Y. Kaneko, S. Nakagawa, Y. Yamaoka, and N. Yamada, "Determination of piezoelectric fields in strained GaInN quantum wells using the quantum-confined Stark effect," Appl. Phys. Lett. **73**, 1691–1693 (1998).
19. B. Gil, O. Briot, and R. L. Aulombard, "Valence-band physics and the optical properties of GaN epilayers grown onto sapphire with wurtzite symmetry," Phys. Rev. B **52**, R17028 (1995).
20. C. Y. Lai, T. M. Hsu, W. H. Chang, K. U. Tseng, C. M. Lee, C. C. Chuo, and J. I. Chyi, "Direct measurement of piezoelectric field in $In_{0.23}Ga_{0.77}N$/GaN multiple quantum wells by electrotransmission spectroscopy," J. Appl. Phys. **91**, 531–533 (2002).
21. J. Piprek, "Efficiency droop in nitride-based light-emitting diodes," Phys. Status Solidi A **207**, 2217–2225 (2010).
22. R. Lu, Q. Hong, Z. Ge, and S.-T. Wu, "Color shift reduction of a multi-domain IPS-LCD using RGB-LED backlight," Opt. Express **14**, 6243–6252 (2006).
23. C. Jia, T. Yu, H. Lu, C. Zhong, Y. Sun, Y. Tong, and G. Zhang, "Performance improvement of GaN-based LEDs with step stage InGaN/GaN strain relief layers in GaN-based blue LEDs," Opt. Express **21**, 8444–8449 (2013).
24. P.-C. Tsai, Y.-K. Su, W.-R. Chen, and C.-Y. Huang, "Enhanced luminescence efficiency of InGaN/GaN multiple quantum wells by a strain relief layer and proper Si doping," Jpn. J. Appl. Phys. **49**, 04DG07 (2010).
25. D. F. Feezell, J. S. Speck, S. P. DenBaars, and S. Nakamura, "Semipolar $(20\bar{2}\bar{1})$ InGaN/GaN light-emitting diodes for high-efficiency solid-state lighting," J. Disp. Technol. **9**, 190–198 (2013).
26. H. Masui, S. Nakamura, S. P. DenBaars, and U. K. Mishra, "Nonpolar and semipolar III-nitride light-emitting diodes: achievements and challenges," IEEE Trans. Electron Dev. **57**, 88–100 (2010).
27. M. Achermann, M. A. Petruska, D. D. Koleske, M. H. Crawford, and V. I. Klimov, "Nanocrystal-based light-emitting diodes utilizing high-efficiency nonradiative energy transfer for color conversion," Nano Lett. **6**, 1396–1400 (2006).
28. T. Erdem and H. V. Demir, "Color science of nanocrystal quantum dots for lighting and displays," Nanophotonics **2**, 57–81 (2013).
29. H. W. Chen, J. He, and S. T. Wu, "Recent advances on quantum-dot-enhanced liquid-crystal displays," IEEE J. Sel. Top. Quantum Electron. **23**, 1900611 (2017).
30. J.-S. Park, J. Kyhm, H. H. Kim, S. Jeong, J. Kang, S.-E. Lee, K.-T. Lee, K. Park, N. Barange, J. Han, J. D. Song, W. K. Choi, and I. K. Han, "Alternative patterning process for realization of large-area, full-color, active quantum dot display," Nano Lett. **16**, 6946–6953 (2016).
31. H. Keum, Y. Jiang, J. K. Park, J. C. Flanagan, M. Shim, and S. Kim, "Photoresist contact patterning of quantum dot films," ACS Nano **12**, 10024–10031 (2018).
32. F. Gou, E.-L. Hsiang, G. Tan, Y.-F. Lan, C.-Y. Tsai, and S.-T. Wu, "High performance color-converted micro-LED displays," J. Soc. Inf. Disp. **27**, 199–206 (2019).
33. H. Sato, A. Tyagi, H. Zhong, N. Fellows, R. B. Chung, M. Saito, K. Fujito, J. S. Speck, S. P. DenBaars, and S. Nakamura, "High power and high efficiency green light emitting diode on free-standing semipolar $(11\bar{2}2)$ bulk GaN substrate," Phys. Status Solidi (RRL) **1**, 162–164 (2007).
34. A. Tyagi, F. Wu, E. C. Young, A. Chakraborty, H. Ohta, R. Bhat, K. Fujito, S. P. DenBaars, S. Nakamura, and J. S. Speck, "Partial strain relaxation via misfit dislocation generation at heterointerfaces in (Al, In)GaN epitaxial layers grown on semipolar $(11\bar{2}2)$ GaN free standing substrates," Appl. Phys. Lett. **95**, 251905 (2009).
35. J. Song, J. Choi, C. Zhang, Z. Deng, Y. Xie, and J. Han, "Elimination of stacking faults in semipolar GaN and light-emitting diodes grown on sapphire," ACS Appl. Mater. Interfaces **11**, 33140–33146 (2019).
36. J. Song, J. Choi, K. L. Xiong, Y. J. Xie, J. J. Cha, and J. Han, "Semipolar (2021) GaN and InGaN light-emitting diodes grown on sapphire," ACS Appl. Mater. Interfaces **9**, 14088–14092 (2017).
37. B. Leung, D. Wang, Y.-S. Kuo, and J. Han, "Complete orientational access for semipolar GaN devices on sapphire," Phys. Status Solidi B **253**, 23–35 (2016).
38. M.-H. Kim, M. F. Schubert, Q. Dai, J. K. Kim, E. F. Schubert, J. Piprek, and Y. Park, "Origin of efficiency droop in GaN-based light-emitting diodes," Appl. Phys. Lett. **91**, 183507 (2007).
39. Y. C. Shen, G. O. Mueller, S. Watanabe, N. F. Gardner, A. Munkholm, and M. R. Krames, "Auger recombination in InGaN measured by photoluminescence," Appl. Phys. Lett. **91**, 141101 (2007).
40. S.-C. Ling, T.-C. Lu, S.-P. Chang, J.-R. Chen, H.-C. Kuo, and S.-C. Wang, "Low efficiency droop in blue-green m-plane InGaN/GaN light emitting diodes," Appl. Phys. Lett. **96**, 231101 (2010).
41. S. H. Yen, M. C. Tsai, M. L. Tsai, Y. J. Shen, T. C. Hsu, and Y. K. Kuo, "Theoretical investigation of Auger recombination on internal quantum efficiency of blue light-emitting diodes," Appl. Phys. A **97**, 705–708 (2009).
42. E. Kioupakis, Q. Yan, and C. G. Van de Walle, "Interplay of polarization fields and Auger recombination in the efficiency droop of nitride light-emitting diodes," Appl. Phys. Lett. **101**, 231107 (2012).
43. J. Piprek, F. Roemer, and B. Witzigmann, "On the uncertainty of the Auger recombination coefficient extracted from InGaN/GaN light-emitting diode efficiency droop measurements," Appl. Phys. Lett. **106**, 101101 (2015).
44. J.-Y. Lien, C.-J. Chen, R.-K. Chiang, and S.-L. Wang, "Patternable color-conversion films based on thick-shell quantum dots," in *SID Symposium Digest of Technical Papers* (Wiley, 2017), pp. 558–561.
45. F. Gou, E.-L. Hsiang, G. Tan, P.-T. Chou, Y.-L. Li, Y.-F. Lan, and S.-T. Wu, "Angular color shift of micro-LED displays," Opt. Express **27**, A746–A757 (2019).